Experimental Validation of New Creep Failure Model for Stainless Steel 304 and Comparison with Established Models

Mohsin Sattar

mohsin.sattar@fs.cvut.cz

Czech Technical University in Prague

Jan Hosek

Czech Technical University in Prague

Sarka Nemcova

Czech Technical University in Prague

Krzysztof Skrzypkowski

AGH University of Krakow

Krzysztof Zagórski

AGH University of Krakow

Uliana Finaeva

Czech Technical University in Prague

Maaz Akhtar

Imam Mohammad Ibn Saud Islamic University

Muhammad Muzamil

NED University of Engineering and Technology

Asad A. Zaidi

Islamic University of Madinah

Research Article

Keywords: creep experiment testing, model validation, Kachanov-Rabotnov model, damage evolution, Norton Bailey model, finite element modelling

Posted Date: May 7th, 2025

DOI: https://doi.org/10.21203/rs.3.rs-6573563/v1

Additional Declarations: No competing interests reported.

Experimental Validation of New Creep Failure Model for Stainless Steel 304 and Comparison with Established Models

Mohsin Sattar [1,*], Jan Hosek [1], Sarka Nemcova [1], Krzysztof Skrzypkowski [2], Krzysztof Zagórski [3], Uliana Finaeva[1] Maaz Akhtar [4], Muhammad Muzamil [5] and Asad A. Zaidi [6]

[1]Faculty of Mechanical Engineering, Czech Technical University in Prague, Technicka 4, 16607 Praha, Czech Republic; jan.hosek@fs.cvut.cz; sarka.nemcova@fs.cvut.cz; uliana.finaeva@fs.cvut.cz
[2]Faculty of Civil Engineering and Resource Management, AGH University of Krakow, Mickiewicza 30 Av., 30-059 Kraków, Poland; skrzypko@agh.edu.pl
[3]Faculty of Mechanical Engineering and Robotics, AGH University of Krakow, Mickiewicza 30 Av., 30-059 Kraków, Poland; zagkrzys@agh.edu.pl
[4]College of Engineering, Mechanical Engineering Department, Imam Mohammad Ibn Saud Islamic University, Riyadh 11432, Saudi Arabia; maakhtar@imamu.edu.sa
[5]Department of Mechanical Engineering, NED University of Engineering and Technology, Karachi, Pakistan; muzamil@neduet.edu.pk
[6]Mechanical Engineering Department, Faculty of Engineering, Islamic University of Madinah, Al Madinah Al Munawwara, Saudi Arabia; sali@iu.edu.sa

*Correspondence: mohsin.sattar@fs.cvut.cz (M.S.)

***Abstract*:** The limitations of the existing creep failure models have led to the development of a new approach for creep life prediction. Traditional models such as Norton–Bailey and Omega often fall short in accurately capturing the tertiary phase of creep in engineering materials. Similarly, models like Kachanov–Rabotnov, Theta Projection, and the Sine Hyperbolic methods require detailed material-specific parameters to effectively predict damage. To overcome these challenges, a novel hybrid creep model has been proposed by integrating the Norton–Bailey and Kachanov–Rabotnov formulations. This combined framework harnesses the strengths of both models while compensating for their individual shortcomings. The model was incorporated into the finite element (FE) software ABAQUS through curve fitting—utilizing regression analysis to transition from the baseline Omega model to the Norton–Bailey model. Validation was carried out through a series of experimental tests, including ambient and high-temperature tensile tests, as well as creep tests on stainless steel 304. The results were then compared with finite element creep simulations using dog bone specimens. The new model demonstrated excellent predictive accuracy, outperforming traditional models like Omega and Norton–Bailey, achieving up to 91.79% accuracy in creep strain and creep strain rate over a 1000-hour test and 93.92% accuracy for 336 h test.

Keywords: creep experiment testing, model validation, Kachanov-Rabotnov model, damage evolution, Norton Bailey model, finite element modelling

1. Introduction

Over the years, numerous empirical and theoretical models have been proposed to predict the creep deformation behavior of materials, each claiming a certain level of accuracy. However, these models often depend on idealized assumptions, which limit their effectiveness in precisely forecasting creep behavior

and estimating the remaining service life of engineering components [1]. Currently, advanced creep prediction techniques are predominantly based on five well-established models: Norton–Bailey [2], Kachanov–Rabotnov [3], Omega [4], Theta Projection [5], and the Sine Hyperbolic models [6]. Although each model offers specific advantages, their applicability is often restricted to certain conditions and operating environments. Among these, the Norton–Bailey model—commercially available in the ABAQUS finite element software by Dassault Systèmes—is widely recognized as a benchmark for creep damage assessment [7]. It utilizes a power law relationship to correlate creep strain rate with time to failure, incorporating a material-dependent exponent. However, this model primarily addresses the primary and secondary creep phases and neglects the tertiary phase, focusing only on strain rate during secondary creep for deformation predictions. Furthermore, the material constants it relies upon are temperature-sensitive, leading to noticeable discrepancies in high-temperature predictions when compared with experimental data [8]. The Omega model, standardized in ASME FFS-1 API/579-1 and initially adopted by the American Petroleum Institute and the Materials Properties Council (MPC), also presents limitations [9]. It struggles to estimate fracture strain accurately for in-service components due to insufficient material data at elevated temperatures. Moreover, it lacks the ability to capture pre-existing or progressive damage, such as crack initiation and propagation [10]. Despite these drawbacks, the Omega model performs well in predicting rupture time at lower temperatures, where the deviation between actual and predicted rupture life is minimal. However, it relies heavily on curve fitting for data extrapolation and cannot accurately represent exponential creep behavior, as its parameters are highly dependent on specific material properties [11].

The Kachanov–Rabotnov (KR) model, which employs coupled constitutive equations for creep damage, has shown more promising capabilities in modeling creep behavior. Its damage evolution parameter effectively captures the tertiary phase of creep [12]. However, the model's primary limitation lies in its reliance on numerous material constants, and it does not incorporate the primary creep phase in life prediction [13]. The KR model represents both continuous creep damage and discontinuous plastic deformation at rupture using a continuous damage function, which increases the complexity of implementation in finite element (FE) analysis [14]. In contrast, the Theta Projection (TP) method uses four material constants: the first two control the magnitude, curvature, and shape of the primary creep phase, while the latter two govern the tertiary phase [15]. Although this method can provide accurate results, it depends heavily on extensive empirical data to define a representative curve [16]. This requirement necessitates the generation of multiple curves under varying conditions and demands rigorous extrapolation within curve families to achieve precise fitting [17]. To overcome these limitations, the Sine-Hyperbolic (SH) model was recently introduced [18]. It addresses several drawbacks of earlier models and aligns well with experimental data. While it adopts a conservative stance by depending on specific material properties, it offers improved predictive accuracy over conventional models [19].

In this paper a more robust creep prediction model is being proposed with the conceptual framework by the combination of Norton Bailey and Kachanov Rabotnov models. The objective is integrating these classical models into a more advanced or unified framework to improve predictions or to model more complex material behaviours under various loading conditions [20]. The Norton-Bailey model is typically used in the context of creep deformation in materials under constant stress over time. It is particularly relevant for describing how materials behave under long-term loading, where the deformation happens at a much slower rate compared to instantaneous elastic deformations. It describes the relationship between stress and strain rate in a material undergoing creep. The model is based on a power-law equation and the Norton-Bailey model is commonly used for materials like metals and polymers that undergo time-dependent deformation under constant stress [21]. The Kachanov-Rabotnov model is an extension of the classical creep theory, and it is used to describe damage evolution in materials over time. This model incorporates the idea of damage mechanics, where material degradation due to stress leads to the development of cracks or voids, influencing the material's overall behaviour [22]. This model focuses on damage accumulation and its impact on the material's mechanical properties. It is commonly expressed by a damage variable, which evolves with time and is linked to the applied stress and strain rate [23]. The Kachanov-Rabotnov model is used to predict material failure by considering the degradation of material properties over time. It is particularly relevant for materials that experience damage accumulation under both cyclic and static loading conditions [24].

The goal of combining these two models—Norton-Bailey and Kachanov-Rabotnov—into a new conceptual framework is to create a more comprehensive and accurate representation of material behaviour under stress, accounting for both creep deformation and damage accumulation. The combination would allow for the time-dependent creep and the Norton-Bailey model can be used to capture the slow, time-dependent deformation of materials under constant stress, describing how the material deforms over time. The Kachanov-Rabotnov model can be integrated to represent how the material deteriorates over time, even as it undergoes creep. This is important because as materials deform, they accumulate damage, which can accelerate the creep process or lead to premature failure. The damage evolution could be coupled with the creep deformation rate. For example, the damage variable could influence the creep exponent or the material constant in the Norton-Bailey model [25]. This would allow for a more accurate representation of how material damage accelerates creep deformation over time. As the damage variable increases, the material's stiffness, strength, or resistance to creep could decrease. This means that the material's response to stress becomes more nonlinear as it accumulates damage, leading to a more accurate prediction of failure [26]. The combination of these models could also allow for multi-stage creep behaviour, where the material exhibits different types of creep stages i-e primary, secondary and tertiary stage as it accumulates damage. In the later stages of creep, when damage becomes significant, the material may experience a rapid increase

in strain rate, leading to failure.

In practical terms, the new combined model could be used to better predict, the failure in engineering components: Especially for materials used in high-stress environments, e.g., pressure vessels, turbine blades etc. that experience both long-term loading and damage accumulation [27]. It could assist in selecting materials for applications where both creep and damage play a significant role in failure, such as in high-temperature, high-stress environments. By combining the two models, engineers and researchers can more accurately predict not just the amount of deformation a material undergoes over time but also when and how the material will start to fail due to the accumulation of damage. The new model thus provides a more comprehensive tool for understanding and predicting material behaviour, leading to better design, maintenance, and failure prevention strategies in various engineering fields [28].

2. Conceptual Framework of New Creep Model

The equations from the Norton-Bailey and Kachanov-Rabotnov models, both of which are grounded in creep power laws, are integrated to form the novel mathematical formulation for the creep model. This new creep model is formulated in Equation (1) and further simplified in Equations (2) and (3).

Creep strain rate: $\dot{\varepsilon}_c = A\,\sigma^n + A\,(\frac{\sigma}{1-\omega})^n,$ (1)

$$\dot{\varepsilon}_c = A\,\sigma^n\,[\,1 + \frac{1}{(1-\omega)^n}\,],$$ (2)

$$\dot{\varepsilon}_c = A\,\sigma^n\,[\,\frac{(1-\omega)^n + 1}{(1-\omega)^n}\,],$$ (3)

where t is the time, σ is the stress, and $\dot{\varepsilon}_c$ is the creep strain rate. A and n are material constants, and ω is the present damage, which is also a material constant but varies with time.

The method of integration adapted for the new creep model in Abaqus is by regression analysis [29]. Equation (4) represents the generic energy law regression, while Equation (5) provides the Norton-Bailey equation for comparisons and deducing the variables as follows:

$$y = A'x^B$$ (4)

$$\dot{\varepsilon}_c = A\,\sigma^n$$ (5)

The standard variable (y) and projection response (x) are involved in this equation, where A' stands for the curve measurement and B is the exponent of the analytical variable (x). The Norton-Bailey power law regression in Equation (6) is compared with Equation (7) for stress exponent (n) of creep equation

$$B = \frac{n' \sum(\ln x \ln y) - \sum(\ln x) \sum(\ln y)}{n' \sum[(\ln x)^2] - [(\sum(\ln x)^2]} \quad (6)$$

$$n \frac{n' \sum(\ln \sigma \ln \dot{\varepsilon}) - \sum(\ln \sigma) \sum(\ln \dot{\varepsilon})}{n' \sum[(\ln \sigma)^2] - [(\sum(\ln \sigma)^2]} \quad (7)$$

Likewise, the parameters were found by comparing the curve coefficient A' in Equation (8) with the Norton-Bailey creep parameter A in Equation (9).

$$A' = e^{\frac{\sum(\ln y) - B \sum(\ln x)}{n'}} \quad (8)$$

$$A = e^{\frac{\sum(\ln \dot{\varepsilon}) - n \sum(\ln \sigma)}{n'}} \quad (9)$$

The number of samples are indicated by n', and the independent variables in this equation are x and σ, the dependent variables are y and $\dot{\varepsilon}_c$. Stress is regarded as an independent variable and strain rate as a dependent variable in the regression analysis. The precision of regression affects the selection of the stress range; a more accurate curve fit is produced by the broader stress range in the sample data. Equations (7) and (9), which describe the creep constraint and stress exponent, are modified for the new model's curve fitting by regression into the Norton-Bailey model in Abaqus, yielding Equations (10) and (11) [30]. To facilitate the modeling of material deformation during the tertiary creep stage, the damage evolution parameter is represented by the constant b in these equations.

$$n = \frac{n' \sum(ln \sigma * b)(ln \dot{\varepsilon}) - \sum(ln \sigma * b) \sum(ln \dot{\varepsilon})}{n' \sum[(ln \sigma * b)^2] - [(\sum(ln \sigma * b)^2]} \quad (10)$$

$$A = e^{\frac{\sum(\ln \dot{\varepsilon}) - n \sum(\ln \sigma * b)}{n'}} \quad (11)$$

where, $b = \frac{\{(1-\omega)+1\}}{(1-\omega)}$; ω = damage evolution parameter; n' = sample size

The new model formulated as in Equation (12):

$$\dot{\varepsilon}_c = A \, \sigma^n * b \quad (12)$$

Curve fitting for damage evolution, through creep power laws for deriving constants in the equation for material independency, is applied. The new model was standardized with the help of the Omega model which is a baseline model for this research study. Curve fitting of the new model to the Norton Bailey model is depicted in Figure 1 while calibrating with the Omega model [31].

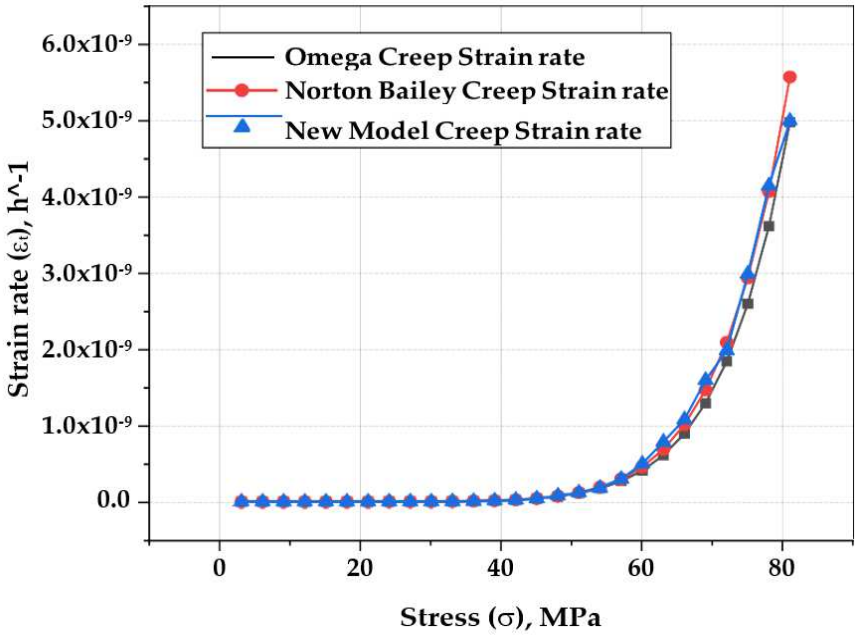

Figure 1. Curve fitting of Omega model to the new model and Norton Bailey model based on strain hardening

3. Materials and Methods

This section outlines the process used to initially determine the analytical creep strain and creep strain rate through regression analysis, utilizing the Omega-Norton Bailey regression models [32]. The implementation of the new creep model is then adapted in ABAQUS by regression analysis as depicted in the following flowchart of Figure 2:

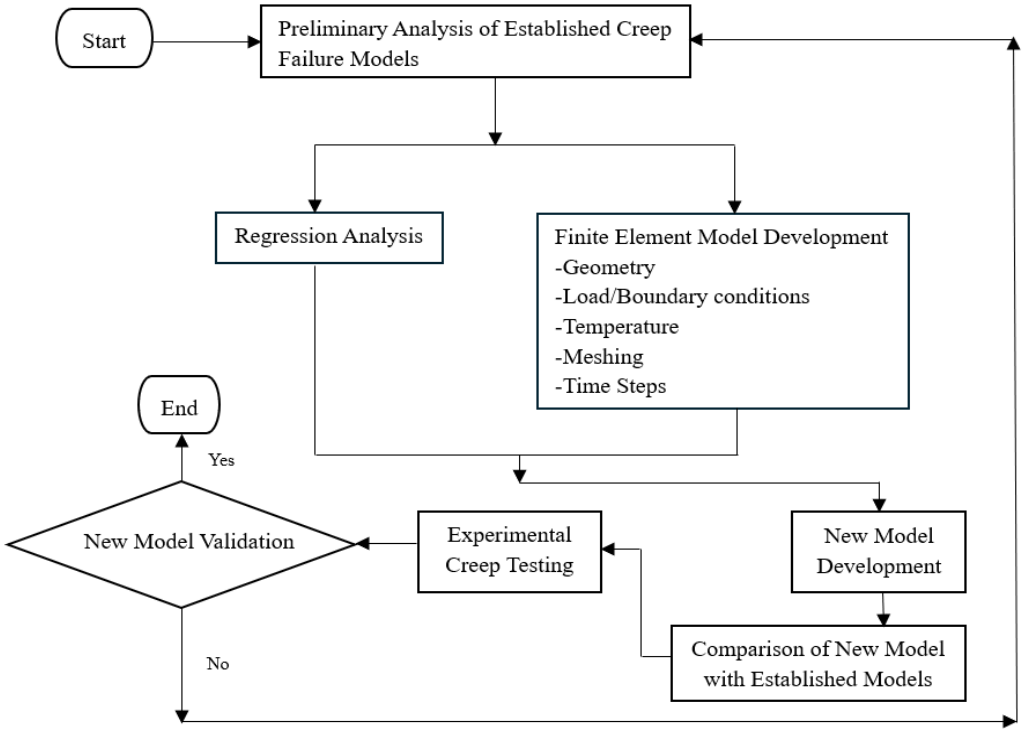

Figure 2. Methodological flowchart for creep model validation

3.1 Material Configuration of Stainless Steel 304

Stainless Steel 304 is an austenitic stainless steel and one of the most widely used stainless steel grades due to its excellent corrosion resistance, formability, and weldability. It is primarily composed of iron, chromium, and nickel, with minor additions of other elements that enhance its mechanical and corrosion-resistant properties [33]. The microstructure of SS-304 is face-centered cubic (FCC), typical of austenitic stainless steels. This phase remains stable at all temperatures, providing excellent toughness even at cryogenic temperatures. The following is the chemical composition tabulated in Table 1 of stainless steel 304 selected for dog bone sample coupons on which experimental testing was carried out for this research study [34].

Table 1. Chemical Composition of Stainless Steel 304

%	C	Mn	Si	P	S	Cr	Ni	N
Min						18	8	
Max	0.08	2.0	0.75	0.045	0.030	20.	10.5	0.10

3.2 Regression-Based Modeling and Extrapolation of Creep Curves for Established Models

The MPC Omega model is widely used for inelastic analysis within the API 579-1/ASME FFS-1 standards for creep evaluation. To analyze the relationship between independent and dependent variables, regression analysis was employed. Curve fitting serves as an effective method for minimizing the volume of data required, making it a valuable tool in modeling creep behavior [35]. When working with experimental or simulated creep data, two main approaches are used to reduce the dataset. The first approach, known as *time hardening*, maintains constant time intervals while measuring strain at various stress levels. The second approach, *strain hardening*, records the time required to reach predetermined strain levels [36].

In the Omega model, the strain rate is dependent on both stress and temperature. By treating temperature as a constant, the strain rate can be approximated using the Norton–Bailey model. Since the Norton–Bailey model is grounded in the power law of creep, the general power law regression equation was also applied for comparison. In this regression analysis, stress was treated as the independent variable, while strain rate served as the dependent variable. The accuracy of the regression was influenced by the selected stress range, with a wider range yielding a better fit. Therefore, curve fitting was carried out across various loads and temperatures for different creep models [37]. For predictive analysis, extrapolation was based on the assumption that the observed material behavior would persist over time. To calculate creep parameters and stress exponents for each model examined in this study, regression equations (7) and (9) established in previous sub-section were utilized. Additionally, a damage evolution parameter (ω) was introduced to represent the progression of tertiary creep damage. This enhancement enabled the modeling of a complete creep curve—encompassing the primary, secondary, and tertiary stages—for stainless steel materials [38]. The Theta Projection, Kachanov–Rabotnov, and Sine-Hyperbolic creep damage models were curve-fitted to the Norton–Bailey model within the ABAQUS environment, while a finite element (FE) model based on a dog-bone geometry was developed for creep analysis.

3.3 Geometric Configuration and Pre-Processing for the Development of Finite Element Model

A finite element (FE) model of a dog-bone-shaped specimen was developed in accordance with ASTM E-139 standards for tensile creep testing [39]. The boundary conditions from the corresponding experimental creep test were applied to the FE model. A reference point was designated to define the direction of displacement during loading. The analysis involved up to 45 increments with a time step totaling 18,000 hours [40]. The model aimed to predict the behavior of stainless steel under constant stress within the elastic limit at both room and elevated temperatures. To achieve this, a combination of plasticity and creep effects was analyzed across various conditions using established creep models. Plastic hardening data was also extracted from the simulation for further evaluation. The results from the different creep models were then compared to identify their limitations under varying conditions. Initially, creep behavior

was modeled using the Norton-Bailey model from the ABAQUS material library [41]. Stainless steel SS-304, assumed to be isotropic, was selected for the study based on analytical assumptions.

A uniaxial force was applied to the specimen under defined boundary conditions, and a thermal field was introduced. An elastic-perfect plastic material model was used to simulate the combined effects of elasticity, plastic deformation, and plasticity [42]. Displacement was measured at one end of the specimen—where a displacement amplitude of 2 mm/min was applied—while the opposite end was fixed. The thermal environment was simulated by applying a temperature field ranging from 0°C to 700°C throughout the SS-304 model. Once the target temperature was achieved, a constant longitudinal load was applied to initiate dislocation and distortion within the grain structure of the material [43]. The load, equivalent to 35% of the ultimate tensile strength (UTS), was maintained until either the test duration was completed or the specimen failed. Throughout the test, data on temperature, load, and elongation was continuously monitored and recorded to ensure consistency. The model was created in ABAQUS, adhering strictly to ASTM standards, dimensions and model geometry as illustrated in Figures 3 (a) and (b) [44].

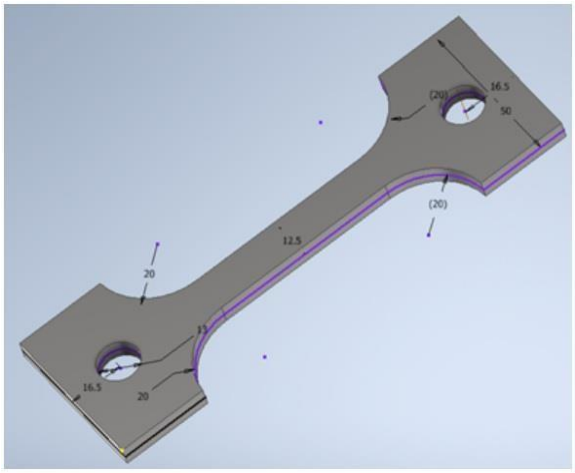

Figure 3. (a) FE geometry of the specimen (in mm) (b) Sample photo of the specimen (in mm)

The physical properties of the isotropic material SS-304, including Young's modulus and Poisson's ratio, were sourced from the ASME BPVC Section II, Part D, Subpart 2 standards [45-46]. These values, relevant to elasticity, are temperature-dependent and are presented in Table 2. It is important to note that Young's modulus exhibited a consistent decline with increasing temperature as depicted in Figure 4(a). Similarly, data related to yield stress and plastic strain, essential for plasticity analysis, were also obtained from the same ASME standards [47], accounting for temperature variations as depicted in Figure 4(b). These standard values, established through rigorous evaluations, reflect the material's response under varying temperatures, pressures, and operating conditions [48].

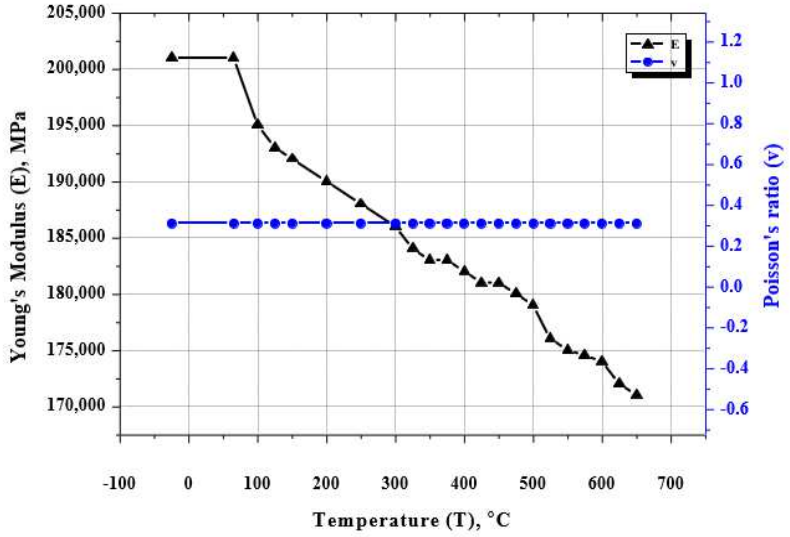

Figure 4. (a) Physical properties of isotropic material SS-304 [47]

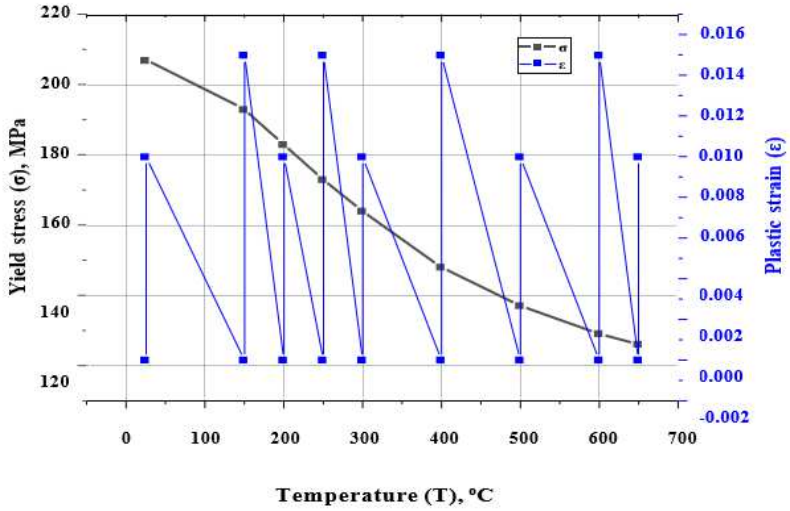

Figure 4. (b) Material properties of SS-304 (isotropic material) [47]

4. Results and Discussions

4.1 Logical Results of Established Creep Failure Models

The analytical results for the established creep failure models were initially derived through regression analysis and curve fitting, using the Omega model as the reference baseline. Figure 5(a) represents the statistically obtained creep strain rate data for Norton-Bailey, Kachanov-Rabotnov, Theta Projection, and Sine Hyperbolic models [49]. The evaluation was performed under consistent physical conditions for Stainless Steel 304, specifically at a temperature of 720 ^{0}C and a time duration of 18,000 hours. Figure 5(b) illustrates the comparative creep strain behavior of these established models under the same testing conditions [50].

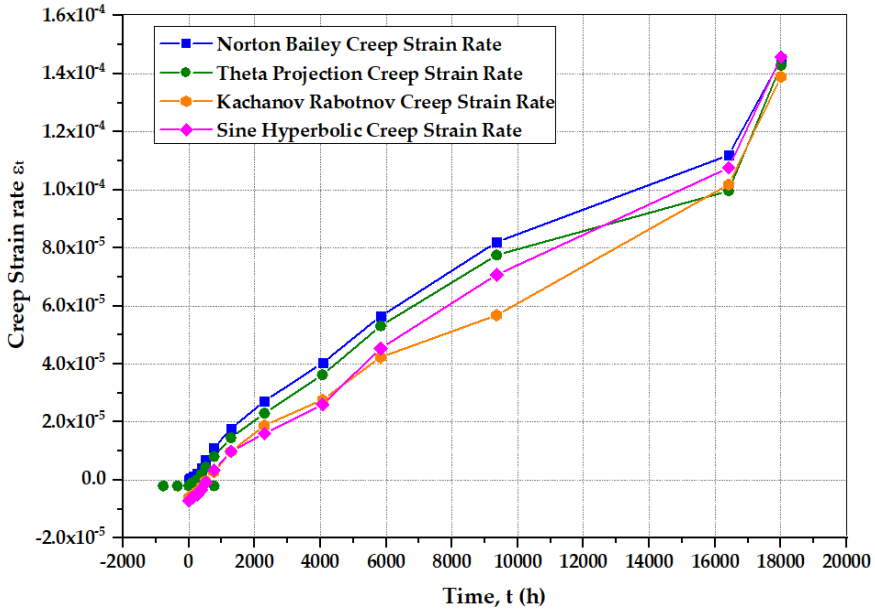

Figure 5(a): Analytical creep strain rates comparison of the established models

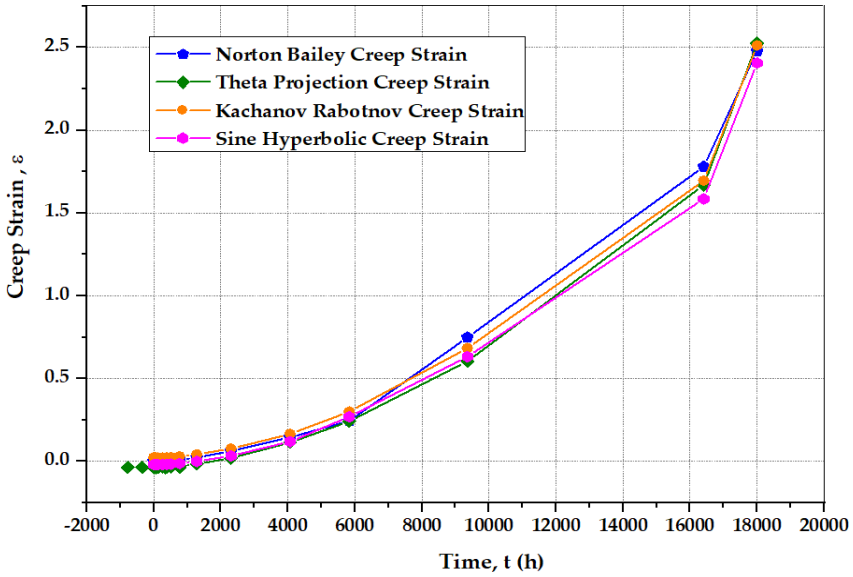

Figure 5(b): Analytical creep strains comparison of the established models

4.2 Finite Element Model Results based on Baseline MPC Omega Model

The finite element (FE) model results were first generated using the MPC Omega model, as it serves as the baseline for standardizing and comparing the other creep models. To simulate the Omega model behavior, relevant parameters such as the stress exponent, creep constants, and material properties were incorporated into the FE analysis. The specimen, made of Stainless Steel 304, was subjected to uniaxial tensile loading, which led to fracture due to sustained stress exceeding the material's yield strength and ultimate tensile strength. Creep damage was demonstrated through this loading condition [51]. The specimen's lower end was constrained using symmetric boundary conditions, and this region experienced

significant deformation. Over the course of the simulation, the applied stress gradually decreased from 60 MPa to approximately 10 MPa and eventually approached zero. This stress relaxation occurred over the full 18,000-hour viscoelastic-plastic cycle. The reduction in stress was a result of continuous plastic deformation and creep rupture, which induced strain in the material. Consequently, stress relaxation was observed as the specimen underwent progressive creep strain under sustained load [52]. The simulations were carried out using 45 time-step increments, and the progression of creep deformation in the specimen was captured at four key intervals—steps 5, 15, 30, and 45—as shown in Figures 6(a), (b), (c), and (d). The evolution from initial to permanent creep deformation was clearly observable across all creep models. Specifically, the color transformation in the results illustrates this behavior: starting with green at the 5th time step (indicating minimal deformation), transitioning to red at the 15th and 30th steps, and culminating in dark red at the 45th step, representing advanced creep deformation [53].

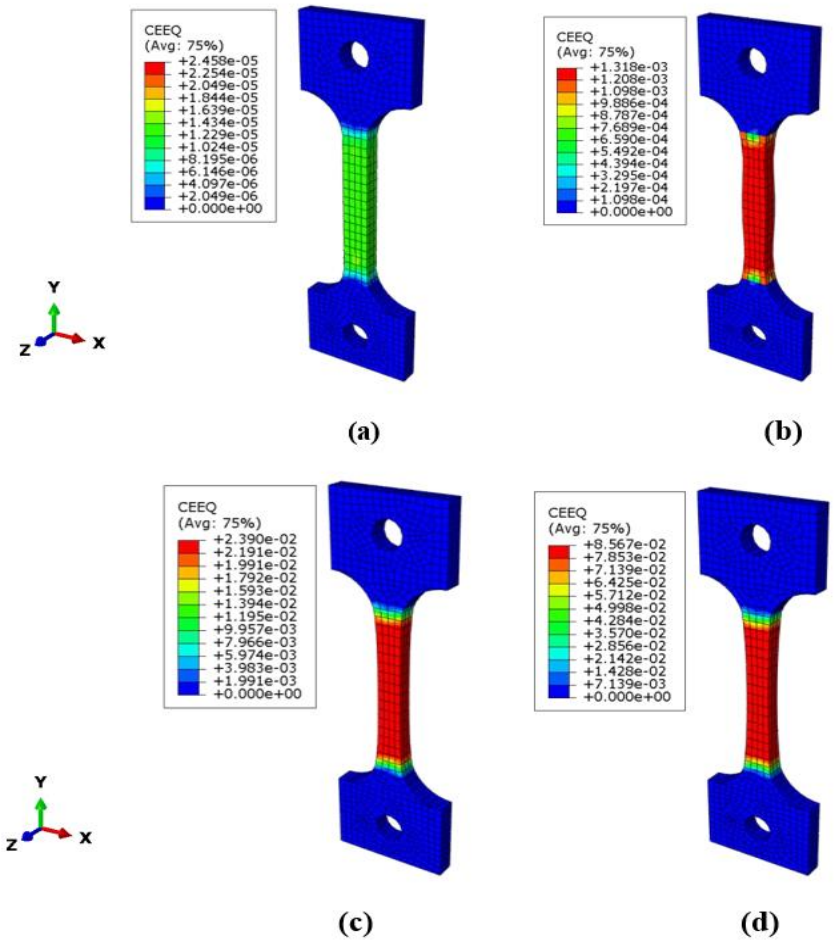

Figure 6. (a) Initial elongation of the specimen under applied load at time increment 5; (b) Onset of primary creep deformation at time increment 15; (c) Development of steady-state (secondary) creep deformation at time increments 30; (d) Accelerated creep deformation and rupture during the tertiary stage at time increment 45.

After running the simulations while utilizing the parameters obtained by implementing the Omega model. The results for creep strain and strain rates are depicted in Figure 7(a) and (b) which were compared with the FE results of the built-in Norton Bailey model [54].

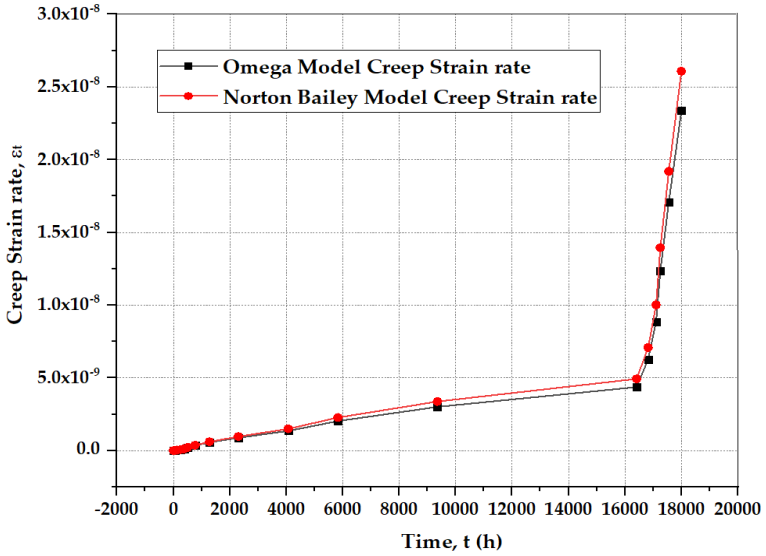

Figure 7.(a) Comparison of Omega and Norton Bailey model's creep strain rate

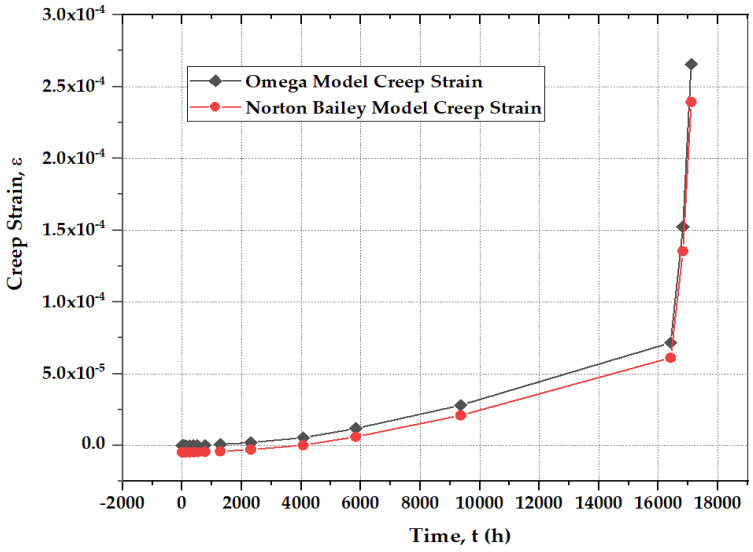

Figure 7.(b) Comparison of Omega and Norton Bailey models creep strain

4.3 Experimental Creep Test Results

Creep test data were experimentally obtained from 11 specimens of SS-304 dog bone sample coupons, which underwent a series of tests including ambient tensile, hot tensile, and creep testing. The ambient and hot tensile tests were conducted to determine the yield strength and ultimate tensile strength of the SS-304 material [55]. The following sub-sections detail the experimental methodology, starting with ambient tensile testing, followed by hot tensile testing, and concluding with the creep test procedures. All tensile tests were carried out in accordance with relevant ASTM standards [56].

4.3.1 Ambient Tensile Tests

Ambient tensile tests were performed on the specimens to evaluate their deformation behavior under load at room temperature. These tests aimed to determine and confirm the yield strength of the SS-304 sample material utilized under ambient conditions. Figure 8(a) represents the tensile stress-strain curves for three specimens 1,2 and 3 tested until rupture, while the variations in yield strength are summarized in Table 2 [57].

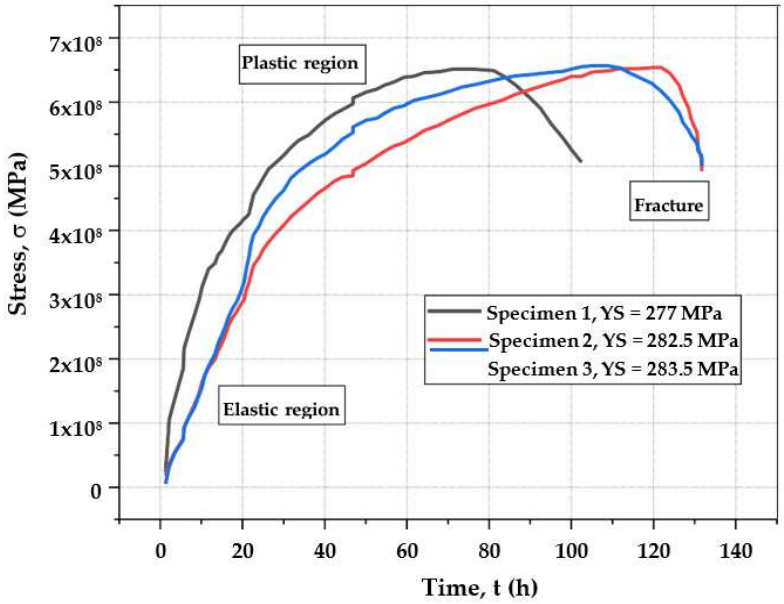

Figure 8. (a) Ambient tensile tests for specimens 1, 2 and 3

Table 2. Test results for ambient tensile test

	Specimen Numbers		
	1	2	3
Elastic Modulus (GPa)	185.5	154.2	132.2
Yield strength (MPa)	277	282.5	283.5
Strain (%)	0.235	0.271	0.319

4.3.2 Hot Tensile Tests

Hot tensile tests were performed at 600 °C and 700 °C using three specimens for each temperature condition to determine and verify the ultimate tensile strength of the SS-304 material, a critical parameter for subsequent creep testing. Figure 8(b) shows the stress-time curves obtained at 600 ^{0}C for samples 4, 5 and 6 while Figure 8(c) presents the corresponding curves at 700 ^{0}C for samples 7, 8 and 9. The variations in ultimate tensile strength at each temperature are detailed in Table 3(a) for specimens 4, 5, and 6 (600 ^{0}C), and Table 3(b) for specimens 7, 8, and 9 (700 ^{0}C) [58].

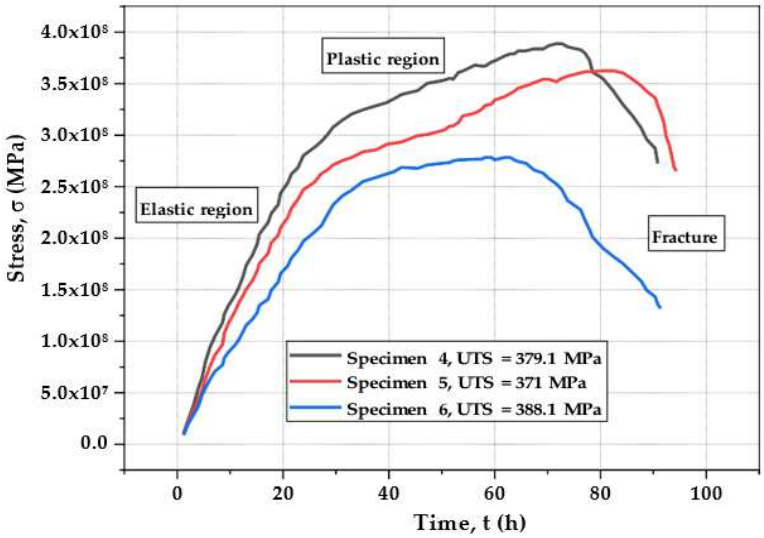

Figure 8. (b) Hot tensile tests for specimens 4, 5, and 6 at 600 ^{0}C

Table 3. (a) Test results for the hot tensile test at 600 ^{0}C

	Specimen Numbers		
	4	5	6
Yield strength (MPa)	150.2	147.3	146.7
Strain (%)	2.41	2.27	2.28
Tensile strength (MPa)	379.1	371	388.1

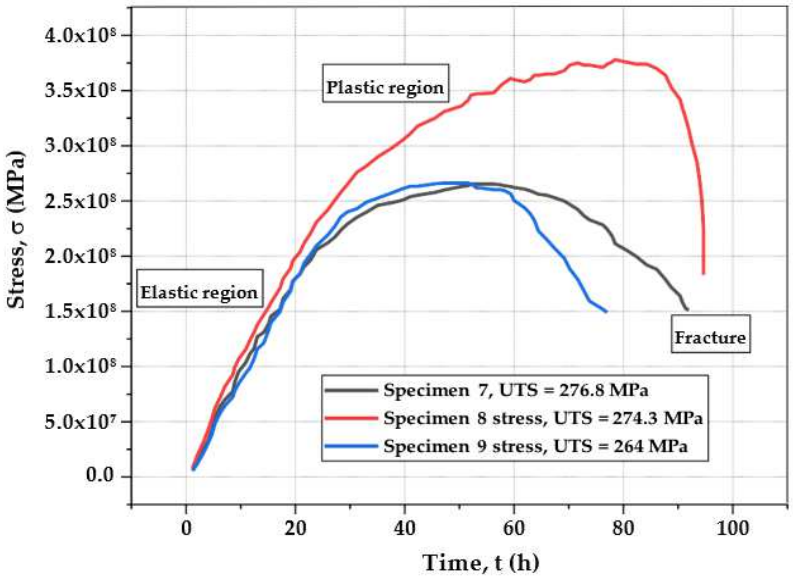

Figure 8. (c) Hot tensile tests for specimens 7, 8, and 9 at 700 ^{0}C

Table 3. (b) Test results for the hot tensile test at 700 ^{0}C

	Specimen Numbers		
	7	8	9
Yield strength (MPa)	122.4	128.1	120.9
Strain (%)	1.97	2.17	1.98
Tensile strength (MPa)	276.8	274.3	264

4.3.3 Creep Tests

The experimental creep test involved a stress-relaxation procedure designed to evaluate the material's deformation behavior over time under constant tensile or compressive load at a fixed temperature. Creep testing is essential for materials intended to operate under sustained loads at elevated temperatures. To assess the creep properties of SS-304, specimens were subjected to two testing durations: a 336-hour (two-week) test and a 1000-hour test. Throughout the tests, crack initiation and propagation were monitored to capture the material's behavior during the primary, secondary, and tertiary stages of creep [59]. The tests were conducted as per ASTM standards to uniformly increase the deformation in time to achieve the induced stress values. Significant material degradation was observed, particularly evident from microstructural deformation. Scanning Electron Microscopy (SEM) analysis revealed grain distortion, elongation, and grain boundary sliding—characteristic signs of advanced creep damage. The tests were conducted at 60% of the material's yield strength, corresponding to 74.28 MPa for the 336-hour test and 52.20 MPa for the 1000-hour test. Testing conditions are summarized in Table 4. The resulting creep curves for the SS-304 specimens are

presented in Figures 9(a) and 9(b), corresponding to the 336-hour and 1000-hour tests, respectively, conducted at 600 ^{0}C and 700 ^{0}C [60].

Table 4. Testing Conditions for Creep Test

Type of Creep Test	Temperature (^{0}C)	Specimens	Loading Conditions	Yield Strength
336 h	600	10	74.28 MPa	60%
1000 h	700	11	52.20 MPa	60%

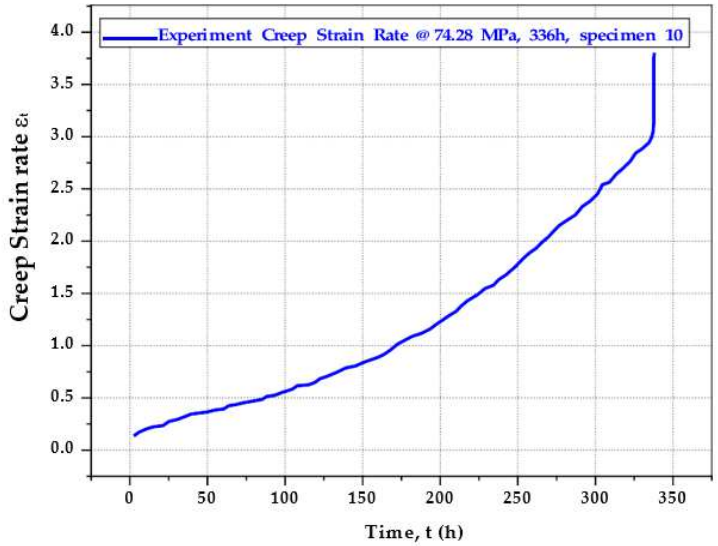

Figure 9. (a) 336 h creep test with loading conditions 60% yield strength (74.28 MPa) at 600 ^{0}C on specimen 10

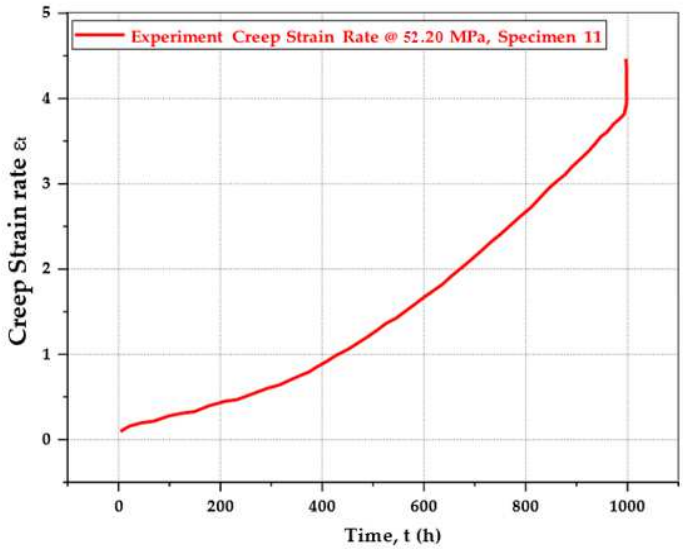

Figure 9. (b) 1000 h creep test with loading conditions 60% yield strength (52.20 MPa) at 700 ^{0}C on Specimen 11

4.4 New Creep Model Validation with Creep Experimental Test Results

For the two-week (336-hour) creep test, a single specimen was tested under conditions of 60% of the material's yield strength, corresponding to a load of 74.28 MPa at 700 °C. The 1000-hour creep test was also conducted at 700 °C, using a lower load of 52.20 MPa, equivalent to 60% of the yield strength under those conditions [61]. All creep testing procedures were carried out in accordance with ASTM E139-11(2018) – Standard Test Methods for Conducting Creep, Creep-Rupture, and Stress-Rupture Tests of Metallic Materials, specifically following the uniaxial tensile creep testing method. Figure 10 shows the mounted specimen after testing, displaying rupture at the center after completing the creep test [62].

Figure 10. Mounted Specimen with Rupture after the Creep Test

Figure 11 illustrates the creep curve obtained from the 1000-hour experimental creep test, compared with the corresponding curves generated through FEA simulations under identical conditions. These simulations were conducted using curve fitting based on the proposed creep material model. Similarly, Figure 12 presents the creep curves from the 336-hour experiment, alongside simulation results using the new creep model [63]. In both cases, comparisons between experimental and simulated results were made under consistent testing conditions. For the 1000-hour test, the creep strain rate obtained through curve fitting yield 91.79% accuracy relative to the experimental data, with a maximum deviation of 5% as tabulated in Table 5. Likewise, for the 336-hour test, the curve fitting method achieved 93.92% accuracy, within a 5% maximum deviation margin, as organized in Table 6. These results confirm that the proposed creep model closely aligns with the laboratory test data, thereby validating its accuracy and reliability [64].

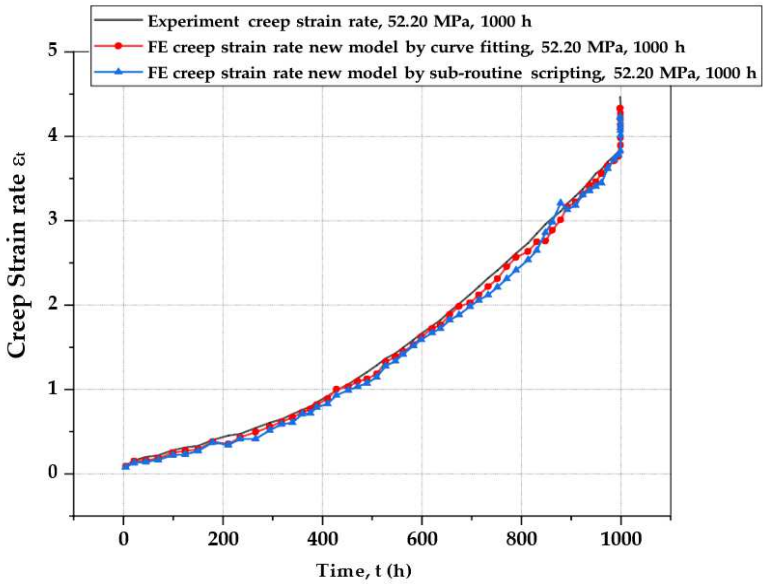

Figure 11. Comparison of predicted creep strain rate by FEA simulation for a new model by curve fitting with experiment creep strain rate at 700 ^{0}C and 1000 h

Table 5. Maximum deviation between Experiment creep strain rate and FE creep strain rate of the new model by curve fitting on selected points for 1000 h test

No. of points	Experiment creep strain rate with a 5% maximum deviation	Experiment creep strain rate	FE creep strain rate of the new model by curve fitting
1	0.290745	0.2769	0.2469
2	0.4712715	0.44883	0.34883
3	0.7916265	0.75393	0.72393
4	1.1102175	1.05735	1.02735
5	1.664208	1.58496	1.52496
6	2.3261595	2.21539	2.11539
7	3.1774995	3.02619	2.882619
8	3.7845885	3.60437	3.55437
9	4.3173375	4.11175	3.981118
10	4.58283	4.3646	4.2646

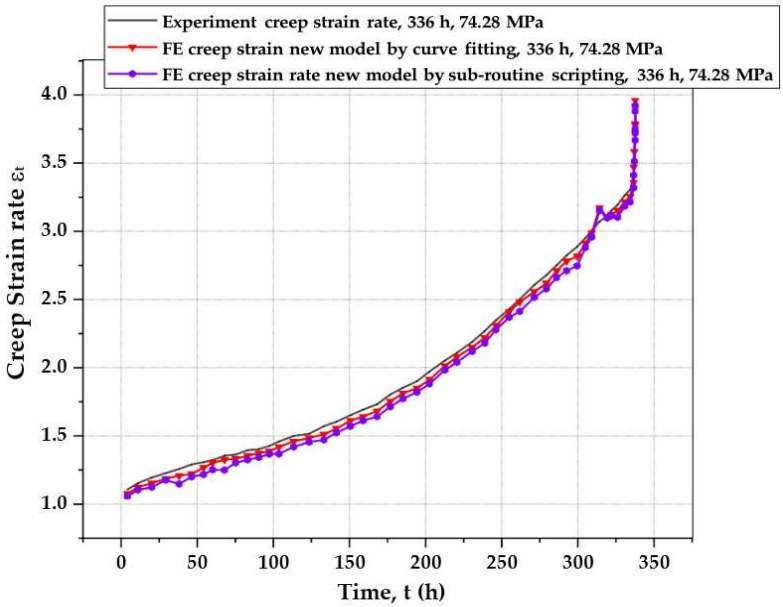

Figure 12. Comparison of predicted creep strain rate by FEA simulation for a new model by curve fitting with experiment creep strain rate at 700 ^{0}C and 336 h

Table 6. Maximum deviation between Experiment creep strain rate and FE creep strain rate of the new model by curve fitting on selected points for 336 h test

No. of points	Experiment creep strain rate with a 5% maximum deviation	Experiment creep strain rate	FE creep strain rate of the new model by curve fitting
1	1.25727	1.1974	1.1574
2	1.468058	1.39815	1.35815
3	1.736952	1.65424	1.61424
4	2.385254	2.27167	2.22167
5	2.55275	2.43119	2.41119
6	2.89001	2.75239	2.71239
7	3.099653	2.95205	2.91205
8	3.268283	3.11265	3.10265
9	3.427799	3.26457	3.21457
10	4.126238	3.92975	3.90975

4.5 Microstructure Examination of the Specimens

Figures 13(a), (b) and Figure 14(a), (b) represent the microscopic analysis of grain structures in the specimens, both before and after undergoing creep tests. Observations from all four cases revealed consistent patterns of grain elongation, distortion, and grain boundary sliding. Notably, the 1000-hour creep test exhibited more pronounced grain deformation compared to the 336-hour test [65]. Grain size measurements highlighted the extent of creep-induced damage, indicating significant changes in the specimen's geometry and grain orientation. These findings suggest that prolonged creep exposure results in severe structural distortion, alterations in crystal lattice dimensions, and a substantial impact on the material properties of SS-304 [66].

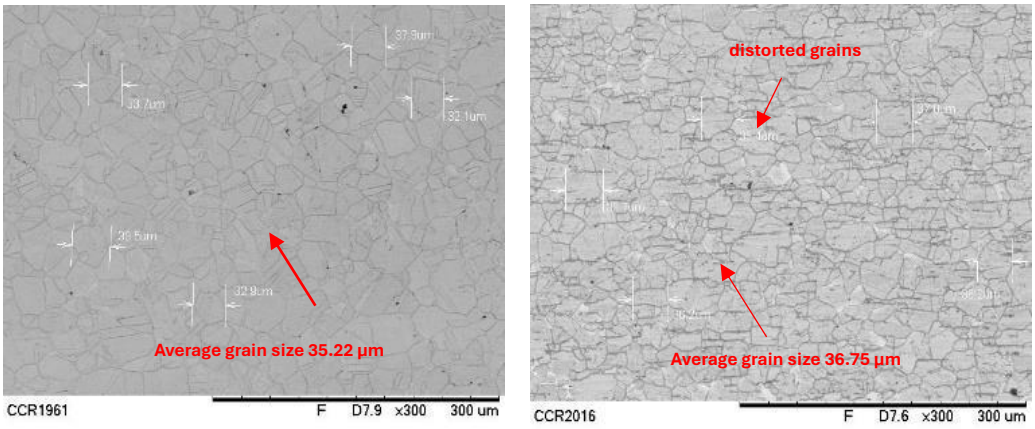

Figure 13. (a) Point of rupture before the creep test (b) Point of rupture after the creep test with grain boundary distortion to 336 h and 700 ^{0}C

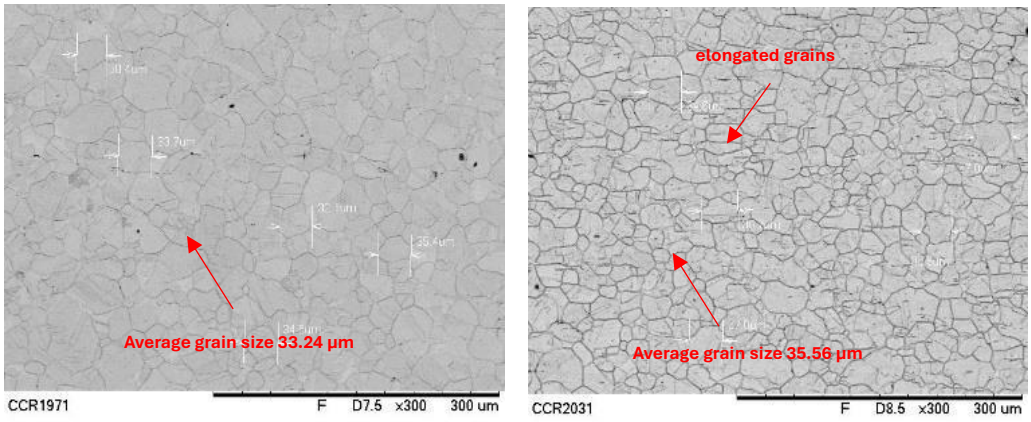

Figure 14. (a) Point of rupture before the creep test (b) Point of Rupture after the creep test with grain boundary sliding up to 1000 h and 700 ^{0}C

4.6 Case Studies Comparisons of Established Models with the New Model

This subsection presents case studies from published literature to benchmark the proposed creep model against established models under identical conditions, thereby evaluating its predictive strength. For instance, Alipour and Nejad [67] applied a modified Theta Projection model to characterize the creep behavior of ferritic steel alloy 2.25Cr–1Mo at an elevated temperature of 754 °C. In a comparable setup, the

newly proposed model was applied to the same material, using material and physical properties sourced from ASME BPVC Section II, Part D [68]. Simulations were conducted using an identical finite element (dog-bone) model with matching geometry, under testing conditions of 754 °C, 110 MPa, and a 300-hour duration. Figure 15 displays the resulting creep curves, while Table 7 presents a comparison at five selected points to assess the model's accuracy against experimental data. The results show that the proposed model achieved an accuracy of 88.5%, compared to 84.3% for the modified Theta Projection model, both within a 5% maximum deviation from the experimental results [69].

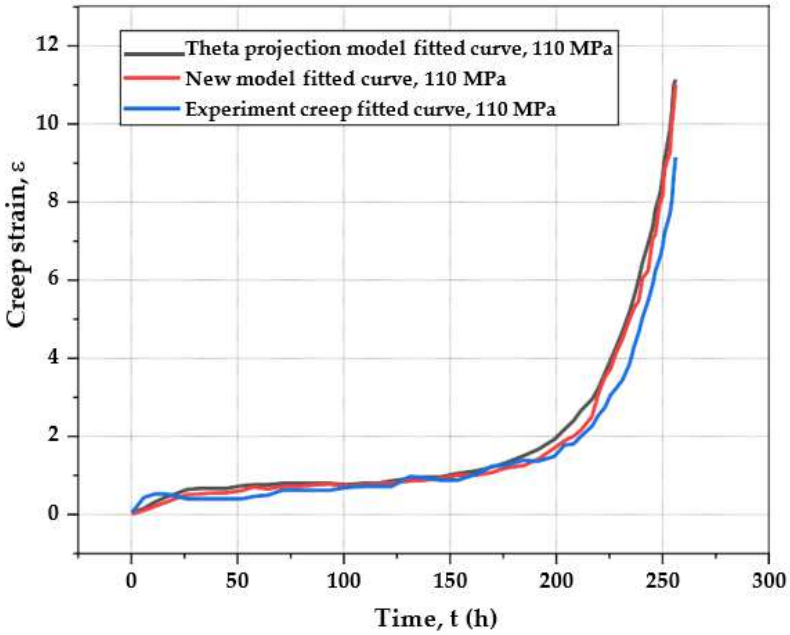

Figure 15. Comparison of the new model and theta projection model FE strain prediction with experiment creep strain for 2.25Cr–1Mo steel, 110 MPa at 754 ^{0}C

Table 7. Comparison of theta projection and new model FE creep strain with experiment creep strain on the selected points

No. of points	Experiment creep strain rate with a 5% maximum deviation	Experiment creep strain	FE creep strain by Theta Projection Model	FE creep strain by New Model
1	0.551891	0.52561	0.44304	0.31304
2	0.652743	0.62166	0.79879	0.758879
3	1.294545	1.23291	1.21604	1.07604
4	3.614174	3.44207	4.68573	4.48573
5	7.55664	7.1968	9.06019	8.800019

In a similar case study, Alipour and Nejad [70] employed the Sine Hyperbolic model to predict the creep behavior of ferritic steel 2.25Cr–1Mo under conditions of 90 MPa and 750 °C, with a test duration of 1000 hours. To evaluate the performance of the proposed model under identical conditions, it was applied to the same material using matching physical parameters. The comparative results are illustrated in Figure 16 and detailed in Table 8. The analysis showed that the proposed model achieved a prediction accuracy of 92%, significantly outperforming the Sine Hyperbolic model, which reached only 72% accuracy against the experimental creep data at selected points [71].

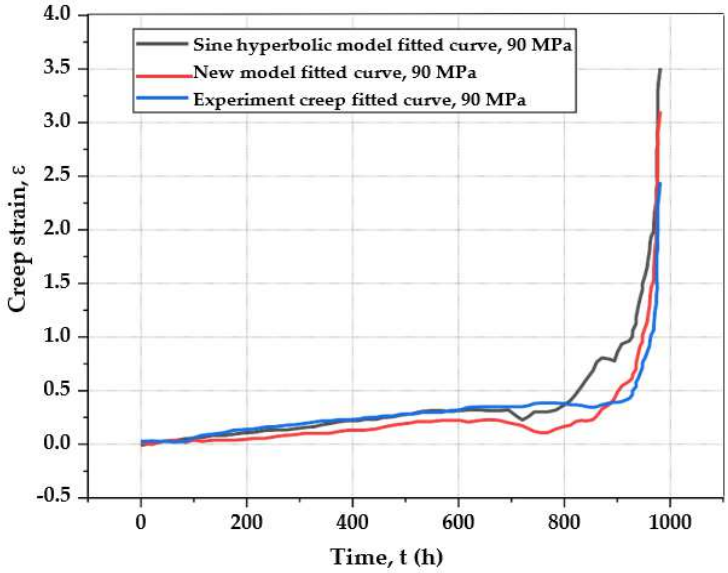

Figure 16. Comparison of the new model and sine hyperbolic model FE strain prediction with experiment creep strain for 2.25Cr–1Mo steel, 90 MPa at 750 ^{0}C

Table 8. Comparison of sine hyperbolic and new model FE creep strain with experiment creep strain on the selected points

No. of points	Experiment creep strain rate with a 5% maximum deviation	Experiment creep strain	FE creep strain by Sine hyperbolic Model	FE creep strain by New Model
1	0.022061	0.02101	0.03513	0.0389
2	0.173859	0.16558	0.13423	0.07353
3	0.277263	0.26406	0.25559	0.17745
4	0.411464	0.39187	0.77777	0.42726
5	1.84589	1.75799	2.74404	2.30608

Another case study involves the application of the Omega model by Manu et al. [72] to evaluate the high-temperature creep behavior of ASME SA-455 steel. Uniaxial finite element analysis was carried out using material constants specific to damage modeling techniques. For comparison, the proposed creep model was also applied to the same material under identical conditions—107 MPa at 720 °C, with a test duration of 1800

hours. Figure 17 and Table 9 present the comparative results between the Omega model and the proposed model at selected data points. The analysis indicates that the proposed model achieved an accuracy of 77.8% in predicting creep strain, outperforming the Omega model, which demonstrated an accuracy of 72.4% under the same conditions [73].

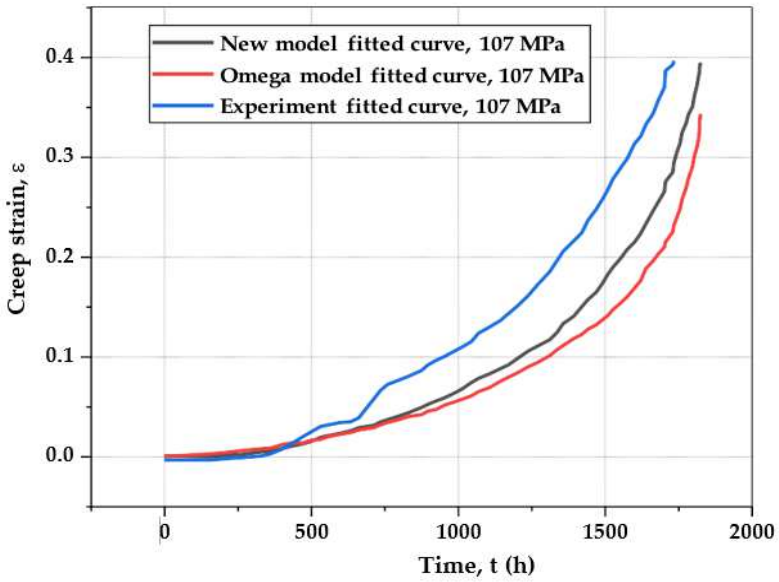

Figure 17. Comparison of the new model and omega model FE strain prediction with experiment creep strain for ASME SA-455 steel, 107 MPa at 720 ^{0}C

Table 9: Comparison of omega model and new model FE creep strain with experiment creep strain on the selected points

No. of points	Experiment creep strain rate with a 5% maximum deviation	Experiment creep strain	FE creep strain by Omega Model	FE creep strain by New Model
1	0.002646	0.00252	0.00075	0.00627
2	0.02729	0.02599	0.03502	0.02429
3	0.067211	0.06401	0.10606	0.0551
4	0.157962	0.15044	0.22463	0.12269
5	0.289412	0.27563	0.3868	0.21525

Finally, a comparison is made between the proposed model and the Kachanov-Rabotnov (K-R) model, which was applied by Haque and Stewart [74] to predict the creep deformation behavior of the superalloy Waspaloy. The tests were conducted at 700 °C, 440 MPa, and lasted up to 3000 hours. The proposed model was applied to the same material, using material and physical properties derived from the ASME BPVC Section II, Part D standards, and implemented in the same finite element (FE) model. Figure 18 presents a comparison between the new model and the K-R model, alongside experimental creep strain data. The results show that the new model achieved 94% accuracy, compared to 92% for the K-R model, both with a 5% deviation from the experimental data at the selected points, as summarized in Table 10 [75].

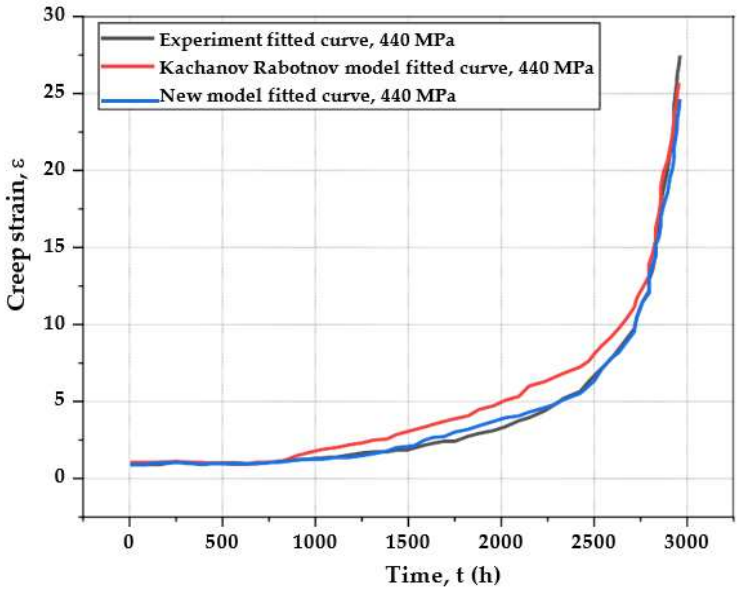

Figure 18. Comparison of the new model and Kachanov-Rabotnov model FE strain prediction with experiment creep strain for superalloy, 440 MPa at 700 ^{0}C

Table 10: Comparison of Kachanov Rabotnov model and new model FE creep strain with experiment creep strain on the selected points

No. of points	Experiment creep strain rate with a 5% maximum deviation	Experiment creep strain	FE creep strain by Kachanov Rabotnov Model	FE creep strain by New Model
1	1.141308	1.08696	1.11441	1.02509
2	1.472856	1.40272	2.01567	1.37423
3	3.538668	3.37016	5.08482	3.94809
4	11.002772	10.47883	11.71028	10.45177
5	22.122429	21.06898	21.46985	19.53742

4. Discussion

The present study experimentally validates a newly proposed creep failure model for Stainless Steel 304 and contrasts its performance with that of well-established models, including the Norton-Bailey and Kachanov Rabotnov relationships. The findings offer insightful contributions to the evolving understanding of creep behavior in austenitic stainless steels and emphasize the predictive capabilities of the new model under various thermal and mechanical conditions.

The newly proposed model demonstrated superior accuracy in predicting creep rupture times across the tested stress and temperature ranges. Unlike traditional models, which often exhibit significant deviations at either high or low stress levels, the new model-maintained consistency in its predictions. This suggests that the formulation effectively captures the dominant mechanisms of creep deformation and damage accumulation in Stainless Steel 304. Comparatively, the Norton-Bailey model, while robust under moderate conditions, showed limitations at elevated temperatures where tertiary creep becomes prominent. The Kachanov Rabotnov model provided reasonable

correlation for rupture strain and life but lacked the flexibility to address microstructural changes influencing the creep rate over long durations. These results align with previous studies that critique the inadequacies of conventional models in accounting for complex metallurgical evolutions, such as grain boundary sliding, carbide precipitation, and void formation during long-term creep exposure [76-78].

The broader significance of these findings lies in their potential impact on the design and life assessment of critical components in power generation, petrochemical, and nuclear industries, where Stainless Steel 304 is commonly employed. By offering a more accurate and comprehensive prediction of creep life, the new model can contribute to improved safety margins, optimized maintenance scheduling, and more efficient material utilization. Moreover, the adaptability of the model to varying loading conditions makes it a strong candidate for integration into finite element analysis (FEA) tools used for creep simulations.

5. Conclusions

This study presented the development and experimental validation of a new creep failure model specifically tailored for Stainless Steel 304. The proposed model was rigorously evaluated through high-temperature creep tests under various stress conditions, and its predictive capabilities were assessed against well-established models, including the Norton-Bailey and Kachanov Rabotnov model approaches.

The key findings from this investigation are as follows:

1. The newly proposed model demonstrated superior accuracy in predicting creep rupture times across a broad range of temperatures and stress levels, as compared to traditional models.
2. Statistical analysis revealed a significantly lower error margin and better correlation coefficients when using the new model, particularly in the tertiary creep region.
3. Unlike generalized models, the proposed formulation effectively captured the specific creep behavior of Stainless Steel 304, indicating the importance of material-specific modeling in high-temperature applications.
4. The model showed consistent performance across multiple test scenarios, confirming its robustness and potential for integration into engineering design tools involving creep life assessments.
5. The creep strain rate obtained by curve fitting and utilizing the new model achieved precision of 91.79% relative to the experimental data for the 1000-hour creep test. Similarly, the creep strain rate obtained by curve fitting and employing the new model achieved accuracy of 93.92% relative to the experimental data for the 336-hour creep test.

In conclusion, the newly developed creep failure model offers a promising alternative for accurately predicting the long-term performance of Stainless Steel 304 under high-temperature conditions. Its enhanced precision and reliability suggest a strong potential for widespread application in industries such as power

generation, petrochemicals, and aerospace, where creep failure remains a critical concern. Future work may explore the model's adaptability to other stainless-steel grades and extend its application to multiaxial stress states and complex loading conditions.

Author Contributions: Conceptualization, M.S, J.H. and S.N.; methodology, M.S, M.A and A.Z.; software, M.S. M.M. and U.F.; validation, M.A., M.M. and S.N.; formal analysis, J.H., K.S., and K.Z.; investigation, A.Z., M.M. and M.A; resources, J.H., S.N. and U.F; data curation, U.F., M.M. and S.N.; writing—original draft preparation, M.S., A.Z., and S.N.; writing—review and editing, M.S., K.S., and K.Z.; visualization, M.A., M.M. and A.Z.; supervision, J.H., K.S., and K.Z.; project administration, J.H., K.S., and K.Z.; funding acquisition, J.H., K.S., and K.Z. All authors have read and agreed to the published version of the manuscript.

Data Availability Statement: The original contributions presented in the study are included in the article, further inquiries can be directed to the corresponding author.

Acknowledgments: The authors would like to gratefully acknowledge the support and facilities provided by the Division of Precision Mechanics and Optics, Faculty of Mechanical Engineering, Czech Technical University in Prague, Czech Republic for the preparation of this publication and financial support by the AGH University of Krakow, Poland.

Conflicts of Interest: The authors declare that they have no known competing financial interests or personal relationships that could have appeared to influence the work reported in this paper.

Abbreviations

The following abbreviations are used in this manuscript:

A	Norton's Power Law Constant
n	Stress Exponent
FFS	Fitness for Service
API	American Petroleum Institute
UTS	Ultimate Tensile Strength
MPC	Material Properties Council
CDM	Continuum Damage Mechanics
ASTM	American Standards for Testing of Materials
KR	Kachanov Rabotnov Model
NB	Norton Bailey Model
SH	Sine Hyperbolic model
ε_t	Creep Strain rate
ε_0	Initial Creep Strain
Ω	Omega material damage constant
ω	Omega damage parameter
ASME	American Society for Mechanical Engineers

References

1 M. Sattar, A.R. Othman, S. Kamaruddin, Maaz Akhtar, Rashid Khan, “Limitations on the computational analysis of creep failure models: A review”, Engineering Failure Analysis, Volume 134, 2022, 105968, https://doi.org/10.1016/j.engfailanal.2021.105968

2 F. Norton, The Creep of Steels at High Temperatures, vol. 1, no. 1, Mc Graw Hill, New York, 1929, p. 90. Author 1, A.; Author 2, B. *Book Title*, 3rd ed.; Publisher: Publisher Location, Country, 2008; pp. 154–196.

3. L.M. Kachanov, Rupture Time under Creep Conditions, Int. J. Fract. 97(1–4) (1999), doi: 10.1023/A:1018671022008.

4. M. Prager, Development of the MPC Omega Method for Life Assessment in the Creep Range, J. Press. Vessel Technol. Trans. ASME 117 (2) (1995) 95–103, https://doi.org/10.1115/1.2842111.

5. W.J. Harrison, P.W.J. Evans, Application of the Theta projection method to creep modelling using Abaqus, Growth (Lakeland) February (2014) 1–15.

6. M.S. Haque, An Improved Sin-Hyperbolic Constitutive Model for Creep Deformation and Damage, p. 84, 2015, [Online]. Available: http://me.utep.edu/ cm Stewart /documents/MSH_MSME_2015.pdf.

7. L. Bråthe, L. Josefson, Estimation of norton-bailey parameters from creep rupture data, Met. Sci. 13 (12) (1979) 660–664, https://doi.org/10.1179/ 030634579790434312.

8. B. Dyson, Use of CDM in Materials Modeling and Component Creep Life Prediction, 2014.

9. D.L. May, A.P. Gordon, D.S. Segletes, The Application of the Norton-Bailey Law for Creep Prediction through Power Law Regression, in: Proceedings of the ASME Turbo Expo, vol. 7 A, 2013, pp. 1–8, doi: 10.1115/GT2013-96008.

10. S. Sarkar, I.V. Singh, B.K. Mishra, A.S. Shedbale, L.H. Poh, Source codes and simulation data for the finite element implementation of the conventional and localizing gradient damage methods in ABAQUS, Data Br. 26 (2019) 104533, https://doi.org/10.1016/j.dib.2019.104533.

11. M.S. Haque, C.M. Stewart, The Disparate Data Problem: The Calibration of Creep Laws across Test type and Stress, Temperature, and Time Scales, Theor. Appl. Fract. Mech. 100 (January) (2019) 251–268, https://doi.org/10.1016/j.tafmec.2019.01.018.

12. C.M. Stewart, A.P. Gordon, Methods to Determine The Critical Damage Criterion of the Kachanov-Rabotnov Law, ASME Int. Mech. Eng. Congr. Expo. Proc., vol. 3, no. PARTS A, B, AND C, pp. 663–670, 2012, doi: 10.1115/IMECE2012-88389.

13. C.M. Stewart, A.P. Gordon, Analytical method to determine the tertiary creep damage constants of the Kachanov-Rabotnov constitutive model, in: ASME, International Mechanical Engineering Congress & Exposition IMECE2010, 2010, pp. 1–8.

14. C.M. Stewart, A.P. Gordon, E.A. Hogan, A. Saxena, Characterization of the creep deformation and rupture behavior of DS GTD-111 using the Kachanov- Rabotnov Constitutive Model, J. Eng. Mater. Technol. Trans. ASME 133(2) (2011), doi: 10.1115/1.4003111.

15. M.S. Haque, C.M. Stewart, Metamodeling Time-Temperature Creep Parameters, J. Press. Vessel Technol. 142 (3) (2020) 1–14, https://doi.org/10.1115/ 1.4045887.

16. R.W. Evans, J.D. Parker, B. Wilshire, The θ Projection Concept-A Model-Based Approach to Design and Life Extension of Engineering Plant, Int. J. Press. Vessel. Pip. 50 (1–3) (1992) 147–160, https://doi.org/10.1016/0308-0161(92)90035-E.

17. Liu, H.; Peng, F.; Zhang, Y.; Li, Y.; An, K.; Yang, Y.; Guan, X.; Zhu, W. A New Modified Theta Projection Model for Creep Property at High Temperature. J. Mater. Eng. Perform. 2020, 29, 4779–4785. https://doi.org/10.1007/s11665-020-04973-w.

18. S.G.R. Brown, R.W. Evans, B. Wilshire, A comparison of extrapolation techniques for long-term creep strain and creep life prediction based on equations designed to represent creep curve shape, Int. J. Press. Vessel. Pip. 24 (3) (1986) 251–268, https://doi.org/10.1016/0308-0161(86)90125-0.

19. C.M. Stewart, A Hybrid Constitutive Model for Creep, Fatigue, and Creep-Fatigue Damage, University of Central Florida, USA, 2013.

20. M.S. Haque, C.M. Stewart, The stress-sensitivity, mesh-dependence, and convergence of continuum damage mechanics models for creep, J. Press. Vessel Technol. Trans. ASME 139(4) (2017), doi: 10.1115/1.4036142.

21. Sattar, M.; Othman, A.R.; Othman, M.F.; Ali, H.T.; Khan, M.K. New Creep Crack Growth Prediction Model for the Life Assessment of Stainless-Steel Material Using Computational Modeling. Metals 2023, 13, 1854. https://doi.org/ 10.3390/met13111854.

22. O. Golan, A. Arbel, D. Eliezer, D. Moreno, The applicability of Norton's creep power law and its modified version to a single-crystal superalloy type CMSX-2, Mater. Sci. Eng. A 216 (1–2) (1996) 125–130, https://doi.org/10.1016/0921-5093(96)10400-7.
23. C.M. Stewart, A.P. Gordon, Y.W. Ma, R.W. Neu, An anisotropic tertiary creep damage constitutive model for anisotropic materials, Int. J. Press. Vessel. Pip. 88 (8–9) (2011) 356–364, https://doi.org/10.1016/j.ijpvp.2011.06.010.
24. R.K. Penny, M.A. Weber, Robust Methods of Life Assessment During Creep, Int. J. Press. Vessel. Pip. 50(1–3) (1992) pp. 109–131, doi: 10.1016/0308-0161(92) 90033-C.
25. Le May, H.C. Furtado, Creep Damage Assessment and Remaining Life Evaluation, Int. J. Fract. 97(1–4) (1999) pp. 125–135, doi: 10.1023/A: 1018396017834.
26. Batsoulas, N.D. Mathematical description of the mechanical behavior of metallic materials under creep conditions. J. Mater. Sci. 1997, 32, 2511–2527.
27. Woodford, D.A. Accelerated high temperature performance evaluation for alloy optimization, embrittlement, and life assessment. In Proceedings of the CORROSION 2005, Houston, TX, USA, 3–7 April 2005; Volume 2005.
28. Kim, M.-S.; Kim, H.-T.; Choi, Y.-H.; Kim, J.-H.; Kim, S.-K.; Lee, J.-M. A New Computational Method for Predicting Ductile Failure of 304L Stainless Steel. Metals 2022, 12, 1309.
29. Zhang, J.; Li, J.; Zan, J.; Guo, Z.; Liu, K. A Creep Constitutive Model, Based on Deformation Mechanisms and Its Application to Creep Crack Growth. Metals 2022, 12, 2179.
30. Sattar, M.; Othman, A.R.; Akhtar, M.; Kamaruddin, S.; Khan, R.; Masood, F.; Alam, M.A.; Azeem, M.; Mohsin, S. Curve Fitting for Damage Evolution through Regression Analysis for the Kachanov–Rabotnov Model to the Norton–Bailey Creep Law of SS-316 Material. *Materials* **2021**, *14*, 5518. https://doi.org/10.3390/ma14195518.
31. Sattar et al., "Development of new creep material model for use through computational modelling for stainless-steel," *Comprehensive Materials Processing (Second Edition),* Elsevier, 2024, pp. 175-184, https://doi.org/10.1016/B978-0-323-96020-5.00254-5.
32. Chen, H.; Zhu, G.; Gong, J. Creep Life Prediction for P91/12Cr1MoV Dissimilar Joint Based on the Omega Method. Procedia Eng. 2015, 130, 1143–1147.
33. Prager M. The omega method – an engineering approach to life assessment. J Press Vessel Technol. 2000;122(3):273–280. doi: 10.1115/1.556184
34. A. Zeman, R. Novotny, O. Uca, V. Krsjak, J. Macak, L. Debarberis, Behavior of cold-worked AISI-304 steel in stress-corrosion cracking process: Microstructural aspects, Applied Surface Science, Volume 255, Issue 1, 2008, Pages 160-163, https://doi.org/10.1016/j.apsusc.2008.05.301.
35. Xiaohui Zhao, Ziwei Li, Bin Yang, Xiaoyu Sun, Guorui Sun, Shupeng Wang, Chao Chen, Microstructure and mechanical properties of 304 stainless steel produced by interpass milling hybrid direct energy deposition-arc, Journal of Materials Research and Technology, Volume 27, 2023, Pages 3744-3756, https://doi.org/10.1016/j.jmrt.2023.10.137.
36. Al-Bakri, A.A.; Sajuri, Z.; Ariffin, A.K.; Razzaq, M.A.; Fafmin, M.S. Tensile and Fracture Behaviour of very thin 304 Stainless Steel Sheet. J. Teknol. 2016, 78, 45–50. https://doi.org/10.11113/jt.v78.9146.

37. Jones, D.P.; Gordon, J.L.; Hutula, D.N.; Banas, D.; Newman, J.B. An elastic-perfectly plastic flow model for finite element analysis of perforated materials. J. Press. Vessel Technol. Trans. ASME 2001, 123, 265–270. https://doi.org/10.1115/1.1357538.
38. L Powers, M.; Arnold, S.M.; Baranski, A. Using ABAQUS Scripting Interface for Materials Evaluation and Life Prediction. In Proceedings of the Abaqus Users' Conference, Cambridge, MA, USA, 23–25 May 2006; pp. 1–11.
39. Jin, Z.H.; Paulino, G.H. Transient thermal stress analysis of an interior crack in functionally graded materials. Am. Soc. Mech. Eng. Aerosp. Div. AD 2000, 60, 121–125.
40. Sattar, M.; Othman, A.R.; Muzamil, M.; Kamaruddin, S.; Akhtar, M.; Khan, R. Correlation Analysis of Established Creep Failure Models through Computational Modelling for SS-304 Material. Metals 2023, 13, 197. https://doi.org/10.3390/met13020197.
41. Booker MK. Use of Generalized Regression Models for the analysis of stress-rupture data, Oak Ridge National Laboratory, Oak Ridge, Tennessee 37830, USA. 1978:pp 459–499.
42. Xiao B, Xu L, Zhao L, et al. Creep properties, creep deformation behavior, and microstructural evolution of 9Cr-3W-3Co-1CuVNbB martensite ferritic steel. Mater. Sci. Eng. A. 2018;711:434–447. doi: 10.1016/j. msea.2017.11.061

43. Sattar, M.; A.R. Othman, Jan Hosek, Bahaa Saleh, Hafiz T. Ali, Sohail Hasnain & Kashif Khan (30 Jan 2025): Sensitivity analysis of steel hole plate by utilizing computational methods and newly developed creep model, Materials at High Temperatures, DOI: 10.1080/09603409.2025.2455525.
44. Manu CC, Birk AM, Kim IY. Uniaxial high-temperature creep property predictions made by CDM and MPC omega techniques for ASME SA 455 steel. Eng. Fail. Anal. 2009;16(4):1303–1313. doi: 10.1016/j.engfailanal.2008.08.005
45. Jones, D.R.H.; Ashby, M.F.; Fifth, M. Power Law Creep Equation Mechanisms of Creep, and Creep-Resistant Materials; Engineering Materials 1, 5th ed.; Elsevier: Edinburgh, UK, 2019.
46. ASME. American Petroleum Institute API-579, Fitness for Service, Operation Manual, 3rd ed.; ASME: Washington, DC, USA. 2016.
47. ASME. ASME Boiler and Pressure Vessel Code An International Code—Section II Part A, 1998; ASME: New York, NY, USA, 2015. https://doi.org/10.1016/B978-032303506-4.10361-X.
48. Haque, M.S.; Stewart, C.M. Modeling the creep deformation, damage, and rupture of Hastelloy X using MPC Omega, theta, and sin-hyperbolic models. In Proceedings of the ASME 2016 Pressure Vessels and Piping Conference, Vancouver, BC, Canada. 17–21 July 2016; Volume 6A, pp. 1–10. https://doi.org/10.1115/PVP2016-63029.
49. Haque, M.S.; Stewart, C.M. Exploiting functional relationships between MPC Omega, Theta, and Sin-hyperbolic continuum damage mechanics model. In Proceedings of the ASME 2016 Pressure Vessels and Piping Conference, Vancouver, BC, Canada. 17–21 July 2016; Volume 6A. https://doi.org/10.1115/PVP2016-63089.
50. Yang, F.Q.; Xue, H.; Zhao, L.Y.; Tian, J. Calculations and modeling of material constants in hyperbolic-sine creep model for 316 stainless steels. Appl. Mech. Mater. 2013, 457–458, 185–190. https://doi.org/10.4028/www.scientific.net/AMM.457-458.185.
51. Golan, O.; Arbel, A.; Eliezer, D.; Moreno, D. The applicability of Norton's creep power law and its modified version to a singlecrystal superalloy type CMSX-2. Mater. Sci. Eng. A 1996, 216, 125–130. https://doi.org/10.1016/0921-5093(96)104.
52. Cedro. V.; Pellicote, J.; Bakshi, O.; Render, M. Application of a modified hyperbolic sine creep rate equation to correlate uniaxial creep rupture data of Sanicro 25 and HR6W. Mater. High Temp. 2020, 37, https://doi.org/10.1080/09603409.2020.1817679.
53. Holmstrom, S.; Auerkari, P. Robust Prediction of Full Creep Curves from Minimal Data and Time to Rupture Model. Energy Mater. 2006, 1, 249–255.
54. Hu, M.; Li, K.; Li, S.; Cai, Z.; Pan, J. Analytical Model to Compare and select Creep Constitutive Equation for Stress Relief Investigation during Heat Treatment in Ferritic Welded Structure. Metals 2020, 10, 688.
55. Sattar, M.; Othman, A.R.; Othman, M.F.; Musa, F. Regression Analysis of Omega Model to Norton-Bailey Law for Creep Prediction in Fitness for Service Assessment of Steel Material. Solid State Technol. 2020, 63, 1228–1239.
56. Eno, D.R.; Young, G.A.; Sham, T.L. A Unified View of Engineering Creep Parameters. In Proceedings of the ASME 2008 Pressure Vessels and Piping Conference, Chicago, IL, USA, 27–31 July 2008; Volume 6, pp. 777–792.
57. Booker, M.K. Use of Generalized Regression Models for the Analysis of Stress-Rupture Data. In Proceedings of the ASME/CSME Pressure Vessels and Piping Conference, Montreal, QC, Canada, 25 June 1978; pp. 459–499
58. Alemayehu, D.B.; Huang, S.J.; Koricho, E.G. Experimental and FEM Analysis of three Carbon steel Characterization under Quasi-Static Strain Rate for Bumper Beam Application. In Proceedings of the 2017 The 2nd International Conference on Precision Machinery and Manufacturing Technology, Kenting, Taiwan, 19–21 May 2017; Volume 123.
59. C.M. Stewart, A.P. Gordon, Constitutive modeling of multistage creep damage in isotropic and transversely isotropic alloys with elastic damage, J. Press. Vessel Technol. Trans. ASME 134(4) (2012), doi: 10.1115/1.4005946.
60. G. Potirniche, Prediction and Monitoring Systems of Creep-Fracture Behavior of 9Cr- 1Mo Steels for Reactor Pressure Vessels, 2013.
61. P. Parameswaran, K.S. Chandravathi, K. Laha, V. Karthik, E. Mohandas, M.D. Mathew, Effect of creep exposure on microstructure and mechanical properties of modified 9Cr-1Mo steel, Procedia Eng. 86 (2014) 116–122, https://doi.org/10.1016/j.proeng.2014.11.019.

62. D. Zhang, J. He, J. Liang, Creep rupture mechanism and microstructure evolution around film-cooling holes in nickel-based single crystal superalloy specimen, Eng. Fract. Mech. 235 (2020) 107187, https://doi.org/10.1016/j.engfracmech.2020.107187.
63. P.A. Gonzalez-Gomez, J. Gomez-Hernandez, J.V. Briongos, D. Santana, Lifetime analysis of the steam generator of a solar tower plant, Appl. Therm. Eng. 159 (May) (2019), p. 113805, doi: 10.1016/j.applthermaleng.2019.113805.
64. E. Sancaktar, H. Jozavi, A.H. El-Mahallawy, N.A. Cenci, Application and limitations of the flexural creep test for polymeric materials, Polym. Test. 7 (1) (1987) 39–58, https://doi.org/10.1016/0142-9418(87)90037-7.
65. T.H. Hyde, B.S.M. Ali, W. Sun, Analysis and design of a small, two-bar creep test specimen, J. Eng. Mater. Technol. Trans. ASME 135(4) (2013), doi: 10.1115/ 1.4025192.
66. J.P. Clech, An extension of the omega method to primary and tertiary creep of lead-free solders, Proc. - Electron. Components Technol. Conf. 2 (2005) 1261–1271, https://doi.org/10.1109/ectc.2005.1441432.
67. R. Alipour and A. F. Nejad, "Creep Behavior Characterization of a Ferritic Steel Alloy based on the Modified Theta-Projection Data at an Elevated Temperature," *Int. J. Mater. Res.*, vol. 107, no. 5, pp. 406–412, 2016, doi: 10.3139/146.111362.
68. P.J. Ennis, Creep and stress rupture testing and evaluation of data, Ref. Modul. Mater. Sci. Mater. Eng. no. December 2016, pp. 0–5, 2016, doi: 10.1016/b978- 0-12-803581-8.03415-9.
69. C.M. Davies, F. Mueller, N.P. O'Dowd, G.A. Webster, Analysis of creep crack initiation and growth in different geometries for 316H and carbon manganese steels, J. ASTM Int. 3(2) (2006) doi: 10.1520/JAI13220.
70. R. Alipour, A. Farokhi Nejad, and H. Nilsaz Dezfouli, "Steady State Creep Characteristics of a Ferritic Steel at Elevated Temperature: An Experimental and Numerical Study," *ADMT J.*, vol. 11, no. 4, pp. 115–129, 2018.
71. S.-T. Tu, K. Zhang, Y.u. Bai, J.-P. Tan, G.-J. Deng, Effect of stress regime-dependent creep behavior on measurement of creep strain rate based on small specimen techniques, Fatigue Fract. Eng. Mater. Struct. 42 (1) (2019) 187–196, https://doi.org/10.1111/ffe.12894.
72. C. C. Manu, A. M. Birk, and I. Y. Kim, "Uniaxial High-Temperature Creep Property Predictions made by CDM and MPC Omega Techniques for ASME SA 455 Steel," *Eng. Fail. Anal.*, vol. 16, no. 4, pp. 1303–1313, 2009, doi: 10.1016/j.engfailanal.2008.08.005.
73. M. Sattar, A.R. Othman, S. Kamaruddin, M. Azad Alam, M. Azeem, "Creep Parameters Determination by Omega Model to Norton Bailey Law by Regression Analysis for Austenitic Steel SS-304", Solid State Phenomena, Vol. 324, pp. 188-197, https://doi:10.4028/www.scientific.net/SSP.324.188
74. M. S. Haque and C. M. Stewart, "Finite-Element Analysis of Waspaloy Using Sinh Creep-Damage Constitutive Model under Triaxial Stress State," *J. Press. Vessel Technol. Trans. ASME*, vol. 138, no. 3, pp. 1–9, 2016, doi: 10.1115/1.4032704.
75. M. Azeem, H.H. Ya, M.A. Alam, T.H. Sultan, M. Ali, M. Sattar, T. Ahmad, H. Hatami, M.R. Sadique, A.A. Mokhtar, M. Mustapha, M.A. Khan, F. Masood, "Macroscale assessment of low-velocity impact on hybrid composite laminates", Material Science and Engineering Technology, 2021, vol. 52, pp. 1101–1111, https://doi.org/10.1002/mawe.202000325
76. D.R. Hayhurst, Use of continuum damage mechanics in creep analysis for design, J. Strain Anal. Eng. Des. 29 (3) (1994) 233–241, https://doi.org/10.1243/ 03093247V293233.
77. D. Barbera, H. Chen, Creep rupture assessment by a robust creep data interpolation using the Linear Matching Method, Eur. J. Mech. A/Solids 54 (July) (2015) 267–279, https://doi.org/10.1016/j.euromechsol.2015.07.003.
78. W.M. Cummings, R.H. King, Extrapolation of creep strain and rupture properties of 1/2 per Cent Cr, 1/2 per Cent Mo, 1/4 per Cent V Pipe Steel, Proc. Inst. Mech. Eng. 185 (1) (1970) 285–299, https://doi.org/10.1243/pime_proc_1970_185_036_02.